Electronic Supplementary Information (ESI)

Phosphaacene as a structural analogue of thienoacenes for organic semiconductors

Kyohei Matsuo,*[a] Rina Okumura,[a] Hironobu Hayashi,[a] Naoki Aratani,[a] Seihou Jinnai,[b] Yutaka Ie,[b] Akinori Saeki [c] and Hiroko Yamada*[a]

[a] Division of Materials Science, Nara Institution of Science and Technology (NAIST), 8916-5 Takayama-cho, Ikoma, Nara, 630-0192, Japan.
[b] The Institute of Scientific and Industrial Research (SANKEN), Osaka University, 8-1 Mihogaoka, Ibaraki, Osaka 567-0047, Japan.
[c] Department of Applied Chemistry, Graduate School of Engineering, Osaka University, 2-1 Yamadaoka, Suita, Osaka, 565-0871, Japan.
[*] E-mail: kmatsuo@ms.naist.jp; hyamada@ms.naist.jp

Table of Contents

1. Instrumentation and materials

All reagents and solvent were purchased from FUJIFILM Wako, Kanoto Chemical, Nacalai Tesque, Tokyo Chemical Industry (TCI), or Sigma-Aldrich, and were used as received. Column chromatography was performed using neutral silica gel 60N (Kanto Chemical) and Florisil (150–250 μm, FUJIFILM Wako). Thin layer chromatography (TLC) was performed on the Merck KGaA 105554 silica gel plates. ^{1}H, ^{13}C, and ^{31}F NMR spectra were recorded using a JEOL JNM-ECX-400P specrtometer and a JNM-ECX500 spectrometer at ambient temperature. Chemical shifts of ^{1}H and ^{13}C signals are quoted to tetramethylsilane (δ = 0.00 ppm) as an internal standard. 85% H_3PO_4 (δ = 0.00 ppm) was used as an external standard in ^{31}P NMR spectra. High resolution mass spectra were collected by a JMS-700 spectrometer (EI) and a Bruker MicroTOF II spectrometer (APCI). Thermogravimetric analysis (TGA) was carried out on a Hitachi STA7200 instrument at a heating rate of 5 °C min^{-1} under N_2 gas flow. The temperature-gradient vacuum sublimation was carried out on an ALS P–100MK3 instrument under high vacuum (2×10^{-3} Pa). UV-Vis absorption spectra were measured using a JASCO UV/Vis/NIR spectrophotometer V-670, and fluorescence spectra were measured using a JASCO PL spectrofluorometer FP-6600. Cyclic voltammetry and differential pulse voltammetry were performed on an ALS 612D electrochemical analyzer. The polarized optical microscope images were obtained using Zeiss Axio Scope.A1 microscope. Out-of-plane XRD measurements of the OFET devices were performed using a Rigaku SmartLab X-ray diffractometer with a Cu-Kα source (λ = 1.5418 Å) in the 2θ scan mode at a fixed incidence angle of 0.58°.

2. Synthesis and characterization

Benzo[*b*]thiophene-2-carbardehyde (5)

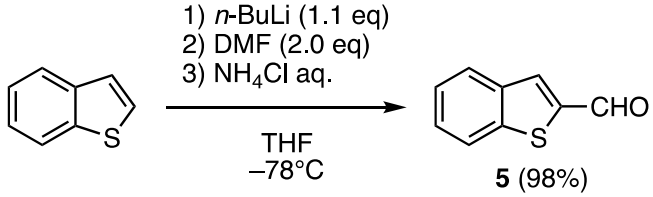

5 (98%)

To a solution of benzo[*b*]thiophene (1.54 g, 11.5 mmol) in dry THF (55 mL) cooled at –78 ºC, *n*-BuLi (1.59 M solution in hexane, 8.0 mL, 12.7 mmol) was added. After 1 h of stirring at –78 ºC, dry DMF (1.8 mL, 23.2 mmol) was added to the reaction mixture. After 2.5 h, the mixture was warmed to room temperature and stirred for 1 h. Next, it was quenched by addition of saturated aqueous NH_4Cl solution. The aqueous phase was extracted with EtOAc and the organic phase was washed with brine, dried over Na_2SO_4 and concentrated. The crude product was purified by column chromatography on silica gel (eluent : EtOAc) to give **5** as yellow oil in 98% yield (1.83 g, 11.3 mmol).

^{1}H NMR (500 MHz, $CDCl_3$): δ = 10.12 (s, 1H), 8.05 (s, 1H,), 7.96 (d, J = 8.0 Hz,1H), 7.91 (d, J = 7.8 Hz, 1H), 7.52 (ddd, J = 7.4, 7.4, 1.6 Hz, 1H), 7.45 (ddd, J = 7.0, 7.0, 1.2 Hz, 1H). HR-MS (EI): *m/z* calcd for C_9H_6OS, 162.0134, $[M]^+$; found 162.0137 (error: 1.85 ppm).

Data is consistent with literature values.[S1]

Bis(benzo[*b*]thiophene-2-yl)methanol (6)

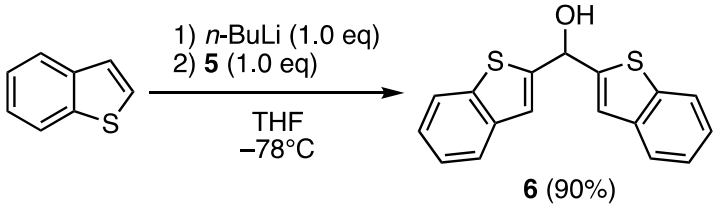

6 (90%)

To a solution of benzo[*b*]thiophene (1.53 g, 11.4 mmol) in dry THF (50 mL) cooled at –78 ºC, *n*-BuLi (1.59 M solution in hexane, 7.1 mL, 11.3 mmol) was added. After 1 h, **5** (1.83 g, 11.3 mmol) dissolved in dry THF (3 mL) was added to the mixture. The solution was held at –78 ºC for 1 h and then allowed to stir at room temperature overnight. Under ambient atmosphere, the solution was quenched with saturated aqueous NH_4Cl solution. The aqueous phase was extracted with EtOAc and the organic phase was washed with brine, dried over Na_2SO_4 and concentrated. The resulting yellow oily solid was washed with hexane to give **6** as a white solid in 90% yield (3.04 g, 10.3 mmol).

^{1}H NMR (500 MHz, $CDCl_3$): δ = 7.81 (d, J = 8.0 Hz, 2H), 7.73 (d, J = 7.5 Hz, 2H), 7.36-7.30 (m, 67H), 6.45 (d, J = 4.0 Hz, 1H), 2.75 (d, J = 4.5 Hz, 1H). HR-MS (EI): *m/z* calcd for $C_{17}H_{12}OS_2$, 296.0324, $[M]^+$; found, *m/z* = 296.0322 (error: –0.68 ppm).
Data is consistent with literature values.[S2]

Bis(benzo[*b*]thiophene-2-yl)methane (2)

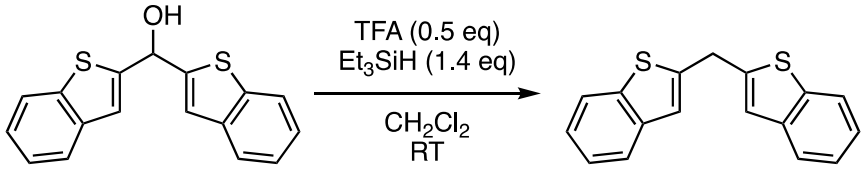

6 **2** (68%)

To a solution of **6** (3.13 g, 10.6 mmol) in dry CH_2Cl_2 (55 mL), trifluoroacetic acid (0.40 mL, 5.23 mmol) and triethylsilane (0.44 mL, 4.70 mmol) were added. After 24 h of stirring at room temperature, K_2CO_3 (2.05 g, 14.8 mmol) was added to the reaction mixture. After 30 min, the reaction mixture was filtered and the filtrate was concentrated to get crude product. The crude product was purified by column chromatography on silica gel (eluent : hexane) to give compound **4** as a white solid in 68% yield (2.00 g, 7.15 mmol).

^{1}H NMR (500 MHz, $CDCl_3$): δ = 7.76 (d, J = 8.0 Hz, 2H), 7.69 (d, J = 7.5 Hz, 2H), 7.32 (ddd, J = 5.5 Hz, 5.5 Hz, 1.0 Hz, 2H), 7.28 (ddd, J = 7.3 Hz, 1.0 Hz, 2H), 7.16 (s, 2H), 4.50 (s, 2H). HR-MS (EI): *m/z* calcd for $C_{17}H_{12}S_2$, 280.0375, $[M]^+$; found, *m/z* = 280.0374 (error: –0.36 ppm).
Data is consistent with literature values.[S2]

Bis(3-bromobenzo[*b*]thiophen-2-yl)methane (3)

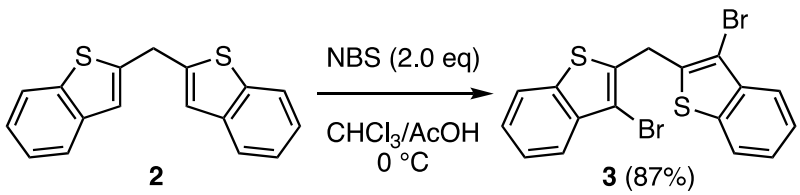

2 **3** (87%)

N-bromosuccinimide (444 mg, 2.49 mmol) was added to ice-cooled solution of **2** (342 mg, 1.22 mmol) in AcOH:$CHCl_3$ (5 mL : 5 mL). The reaction mixture was stirred at 0 ºC for 28 h, and then quenched with saturated aqueous $Na_2S_2O_3$ solution. The organic layer was extracted with CH_2Cl_2, washed with saturated aqueous $NaHCO_3$ solution, water, and

brine and concentrated to give crude product. The crude product was washed with hexane to give compound **3** as white solid in 87% yield (467 mg, 1.06 mmol).

^{1}H NMR (500 MHz, $CDCl_3$): δ = 7.80 (d, J = 8.0 Hz, 2H), 7.72 (d, J = 8.0 Hz, 2H), 7.44 (ddd, J = 8.0 Hz, 8.0 Hz, 1.5 Hz, 2H), 7.36 (dd, J =7.0 Hz, 7.0 Hz, 2.0 Hz, 2H), 4.62 (s, 2H). HR-MS (EI): *m/z* calcd for $C_{17}H_{10}Br_2S_2$ = 435.8585, $[M]^+$; found, *m/z* = 435.8587 (error: 0.46 ppm).

Data is consistent with literature values.[S3]

Compound 1

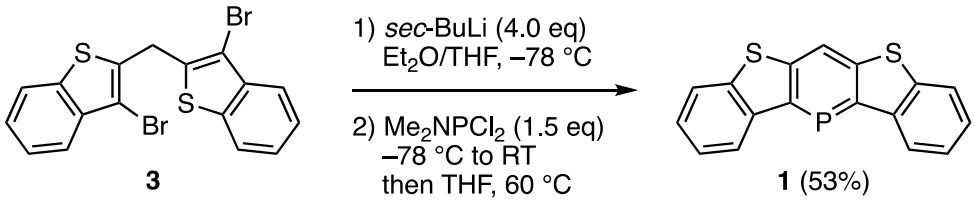

To a solution of **3** (74.9 mg, 0.171 mmol) in dry Et_2O (15 mL) and dry THF (2.5 mL) cooled at –78 ºC, *sec*-BuLi (1.3 M solution in cyclohexane, 0.53 mL, 0.68 mmol) was added. After 20 min, dichloro(dimethylamino)phosphine (0.03 mL, 0.26 mmol) was added and the reaction mixture was stirred at –78 ºC for 1 h. The reaction mixture was warmed to room temperature and stirred for 1 h. The reaction solvent was evaporated and dry THF (17 mL) was added to the reaction mixture and it was stirred at 60 ºC for 2 h. The reaction solvent was evaporated and the resulting product was washed with toluene, and the filtrate was concentrated. The crude product was passed through a short Florisil column (eluent : CH_2Cl_2) and further purified with gel permeation chromatography (eluent : CH_2Cl_2) and washed with hexane to give **1** as yellow solid in 53% yield (28.2 mg, 91.5 μmol).

^{1}H NMR (500 MHz, $CDCl_3$): δ = 8.58-8.57 (m, 2H), 8.50 (d, $J_{H,P}$ = 4.0 Hz, 1H), 7.88 (d, J = 7.5 Hz, 2H), 7.52-7.50 (m, 4H). ^{13}C NMR (126 MHz, $CDCl_3$) : 154.9 (d, J = 47.8 Hz), 143.0 (d, J = 16.9 Hz), 140.6 (d, J = 25.2 Hz), 138.8 (d, J = 10.3 Hz), 127.7 (d, J = 3.0 Hz), 124.7, 122.6, 122.0 (d, J = 14.2 Hz), 119.3 (d, J = 16.9 Hz). ^{31}P NMR (202 MHz, $CDCl_3$); δ = 167.1. HR-MS (APCI): *m/z* calcd for $C_{17}H_{10}PS_2$ = 308.9956, $[M+H]^+$; found, *m/z* = 308.9951 (error: –1.62 ppm).

Compound 4

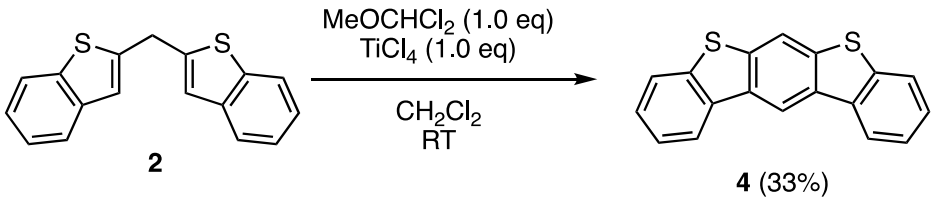

2 **4** (33%)

$TiCl_4$ (0.11 mL, 1.0 mmol) was added to the mixture of dichloromethyl methyl ether (0.09 mL, 1.0 mmol) and **2** (280 mg, 1.0 mmol) in dry CH_2Cl_2 (2.5 mL) at –10 °C. After stirring for 10 min, the mixture was warmed to room temperature and then stirred for 28 h. The reaction mixture was poured onto ice-water, and 2 M HCl was added. It was stirred for 30 min and then transferred to a separation funnel. Organic layer was washed with saturated aqueous $NaHCO_3$ solution, water and brine and dried over Na_2SO_4 and concentrated. The crude product was washed with hexane and further purified with column chromatography on silica gel (eluent : hexane) and gel permeation chromatography to give **4** as white solid in 33% yield (96.7 mg, 0.33 mmol).

^{1}H NMR (500 MHz, $CDCl_3$): δ = 8.90 (s, 1H), 8.31 (dd, J = 7.3 Hz, 1.5 Hz, 2H), 8.28 (s, 1H), 7.87 (dd, J = 6.8 Hz, 1.5 Hz, 2H), 7.54-7.48 (m, 4H). ^{13}C NMR (126 MHz, $CDCl_3$): δ = 139.3, 138.6, 135.2, 133.2, 126.9, 124.5, 122.9, 121.4, 116.1, 113.8. HR-MS (EI): *m/z* calcd for $C_{18}H_{10}S_2$ = 290.0218, $[M]^+$; found, *m/z* = 290.0227 (error: 3.10 ppm).

3. Thermogravimetric analysis

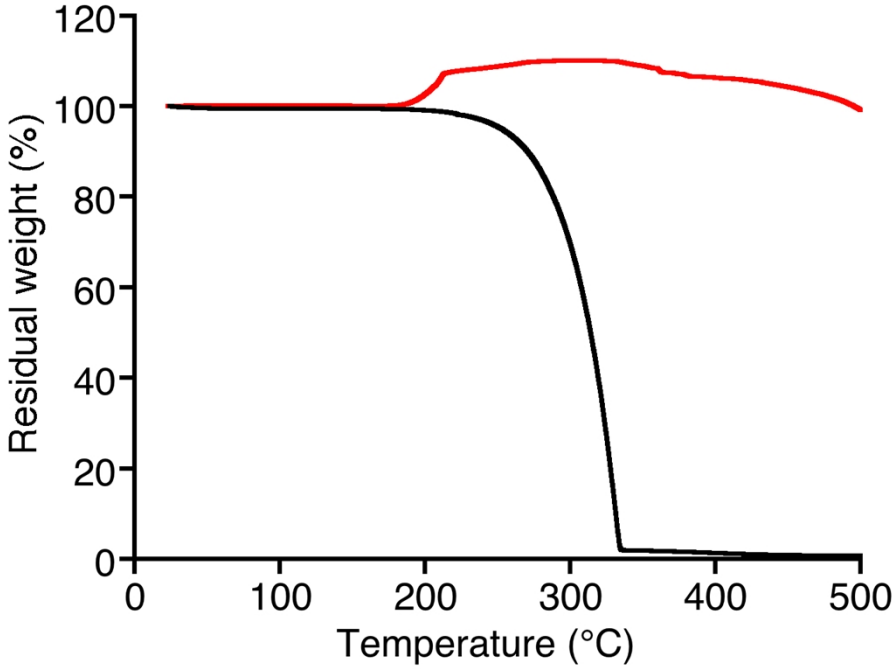

Fig. S1 TGA thermograms of **1** (red) and **4** (black) at a heating rate of 5 °C min^{-1} under N_2 gas flow.

4. X-ray crystallographic analysis

X-ray diffraction data were collected on a Rigaku VariMax RAPID X-ray diffractometer using Mo-Kα radiation (λ = 0.71075 Å) equipped with a large-area IP detector at 103 K. The structure was solved by a direct method (SHELXT-2018) and refined by full-matrix least square method on F^2 for all reflections using SHELXL-2018 program.[S4] All non-hydrogen atoms were refined anisotropically. Hydrogen atoms were placed using AFIX instructions. The crystallographic data have been deposited with the Cambridge Crystallographic Data Centre as supplementary publication materials. These data can be obtained free of charge from the Cambridge Crystallographic Data Centre via www.ccdc.cam.ac.uk/data_request/cif

Crystallographic data for 1

Yellow prism crystals of **1** were obtained by the recrystallization from $CHCl_3$ and heptane using a vapor diffusion method. Total 14081 reflections were collected, among which 2190 reflections were independent (R_{int} = 0.0952). Formula $C_{17}H_9PS_2$; FW = 308.33, crystal size 0.14 × 0.03 × 0.02 mm, Monoclinic, $P2_1/c$ (#14), a = 14.6391(6) Å, b = 3.90201(15) Å, c = 23.5802(10) Å, β = 99.7137(12)°, V = 1327.64(10) Å^3, Z = 4, D_{calcd} = 1.543 g cm^{-3}, R_1 = 0.0441 ($I > 2\sigma(I)$), wR_2 = 0.1084 (all data), GOF = 1.046. CCDC number: 2194939.

Crystallographic data for 4

Colorless prism crystals of **4** were obtained by the recrystallization from $CHCl_3$ and methanol using a vapor diffusion method. Total 18872 reflections were collected, among which 2917 reflections were independent (R_{int} = 0.0906). Formula $C_{18}H_{10}S_2$; FW = 290.38, crystal size 0.17 × 0.10 × 0.01 mm, Orthorhombic, $Pca2_1$ (#29), a = 26.5674(11) Å, b = 3.90265(14) Å, c = 12.4158(5) Å, V = 1287.32(8) Å^3, Z = 4, D_{calcd} = 1.498 g cm^{-3}, R_1 = 0.0473 ($I > 2\sigma(I)$), wR_2 = 0.1081 (all data), GOF = 1.100. CCDC number: 2194940.

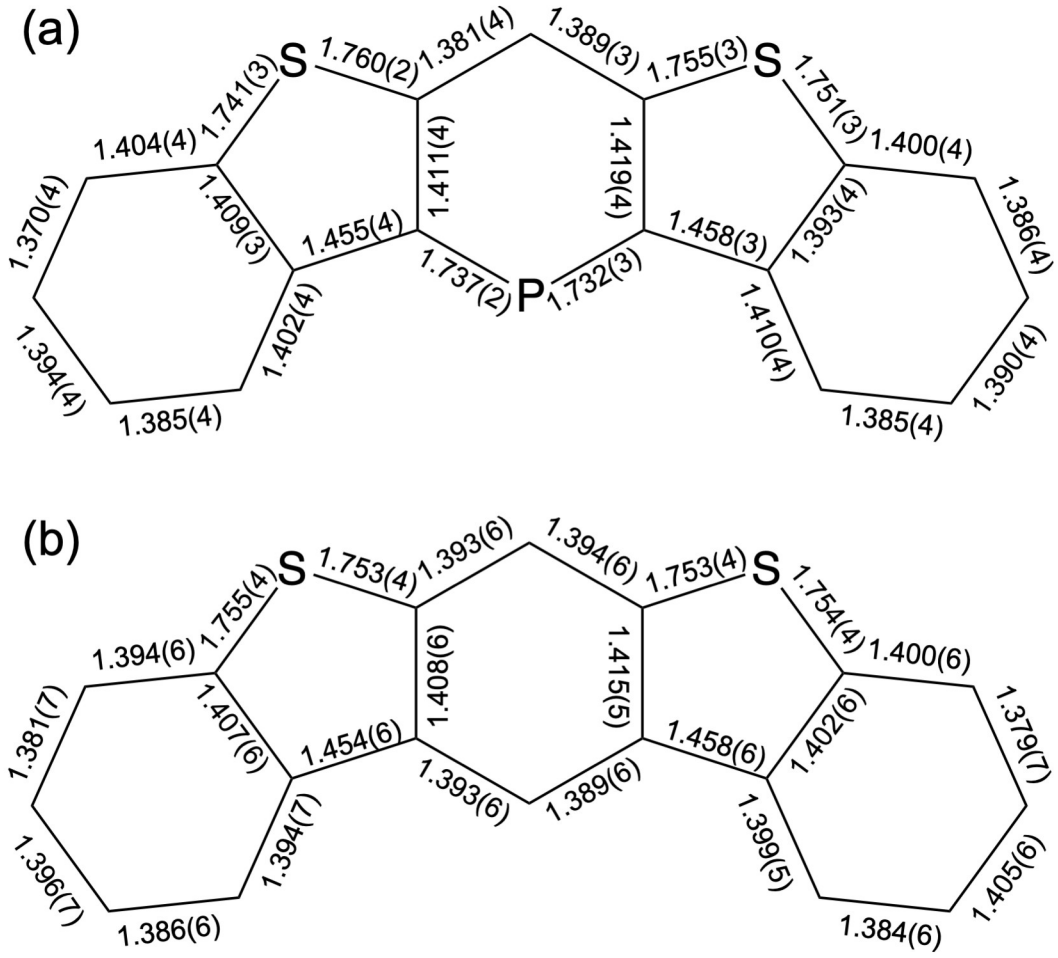

Fig. S2 Bond lengths (Å) of (a) **1** and (b) **4** in the X-ray crystal structure.

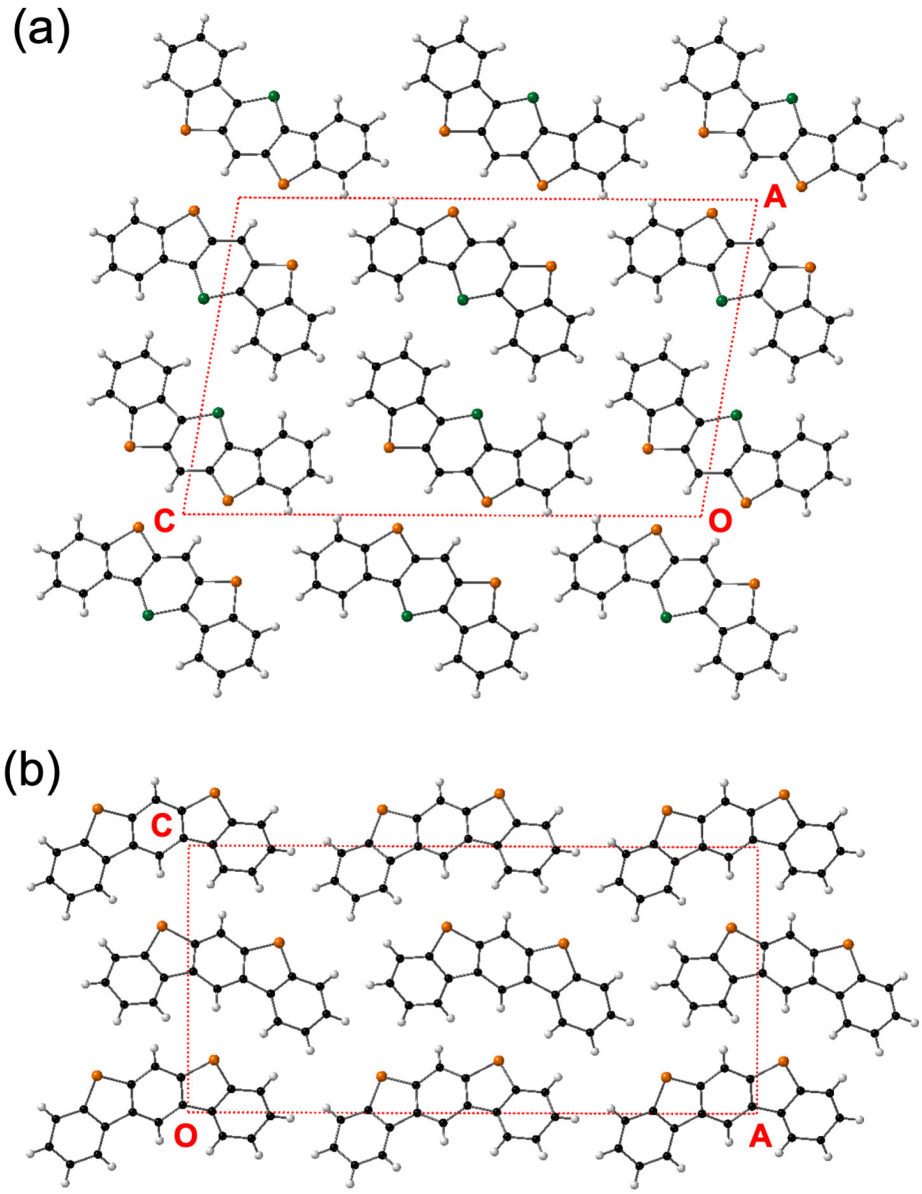

Fig. S3 Packing structures of (a) **1** and (b) **4** viewed along the *b*-axis.

5. Photophysical measurements

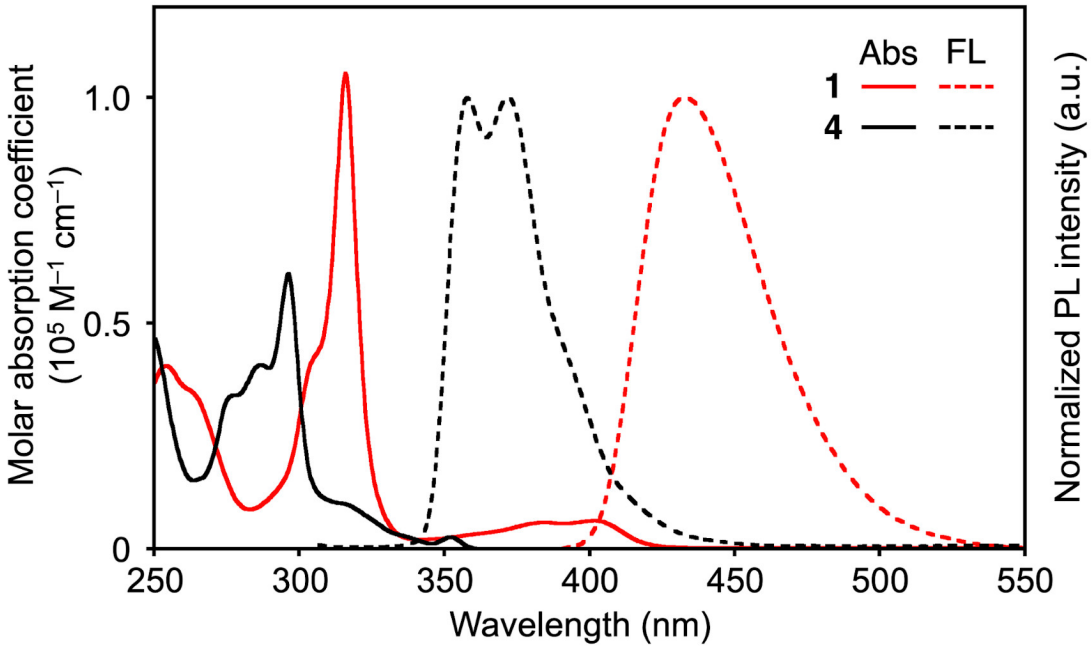

Fig. S4 UV-Vis absorption and fluorescence spectra in chloroform of **1** and **4**.

6. Electrochemical measurements

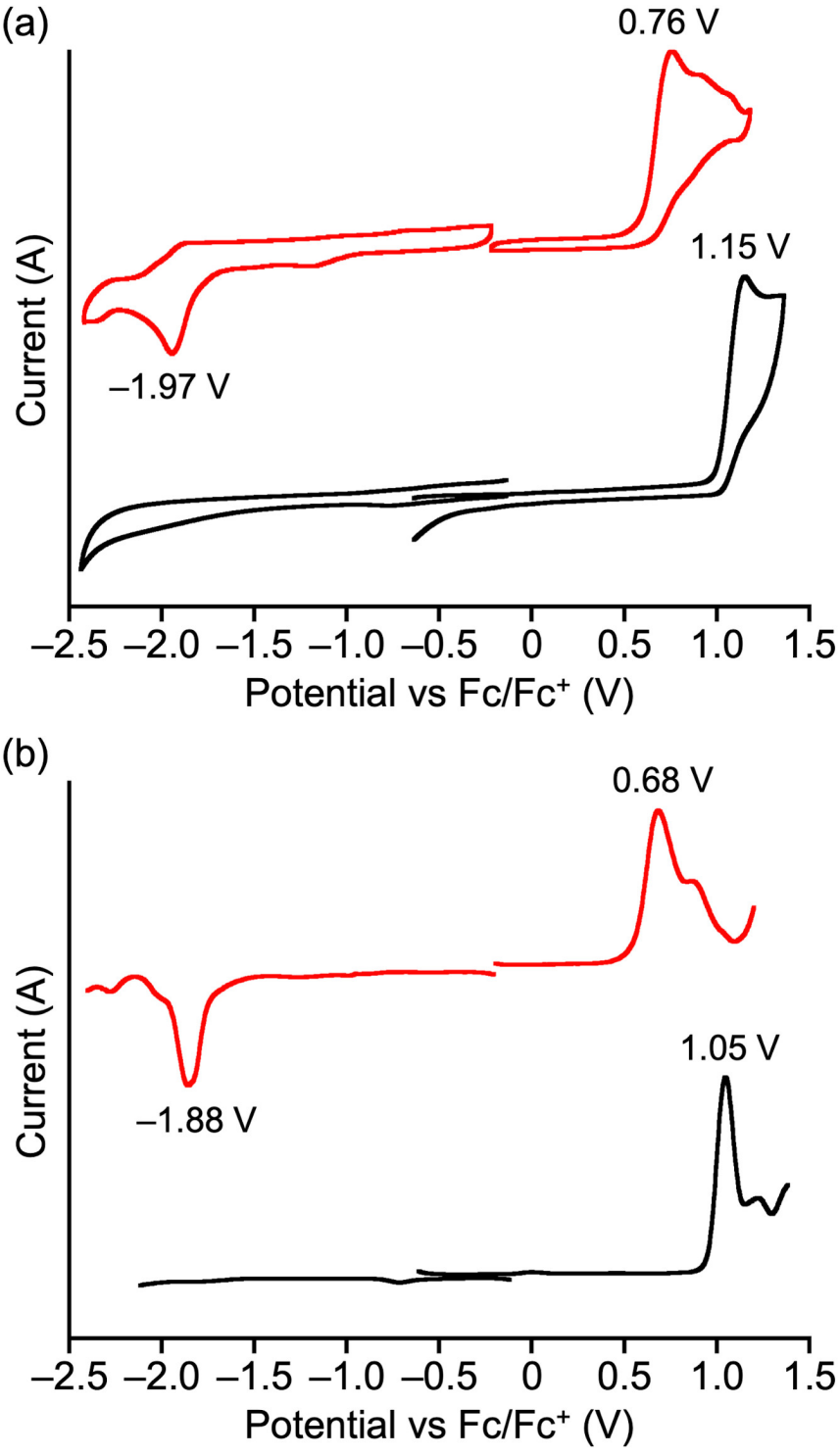

Fig. S5 (a) Cyclic and (b) differential pulse voltammograms of **1** (red) and **4** (black). Solvent: acetonitrile, electrolyte: 0.1 M *n*-Bu_4NPF_6, working electrode: glassy carbon, counter electrode: Pt, reference electrode: $Ag/AgNO_3$, scan rate: 0.1 V s^{-1}.

7. Quantum chemical calculations

The geometry optimizations for **1** and **4** in the ground state were performed using the B3LYP functional with the 6-311G(d,p) basis set in the gas phase, implemented in the Gaussian 16 Revision C.01 program package.[S5] The stationary points were optimized without any symmetry and characterized by frequency calculations at the same level of theory (the number of imaginary frequency was zero). The vertical excitation energies and oscillator strengths of the singlet excited states were calculated by the TDDFT method using the same level of theory. The nucleus-independent chemical shift (NICS)[S6] values were calculated at the B3LYP/6-311G(d,p) level of theory. The reorganization energies for hole transfer (λ_+) and electron transfer (λ_-) were calculated by using a four-point method[S7] (Figure S9) and following equation,

$$\lambda_{\pm} = \lambda_1 + \lambda_2 = (E_0^* - E_0) + (E_{\pm}^* - E_{\pm})$$

where E_0, E_+, and E_- represent the energies of the neutral, cation, and anion species in their optimized geometries, respectively, E_0^* represents the energies of the neutral species in the optimized geometries of the corresponding charged species, and E_+^* and E_-^* represent the energies of the cation and anion species in the optimized geometry of the neutral species, respectively. The geometry optimizations of cation and anion species for **1** and **4** were performed at the UB3LYP /6-311G(d,p) level of theory.

Charge transfer integrals in the crystal packing structures of **1** and **4** were calculated using the ADF2020 program[S8] at the PBE/TZ2P level of theory.

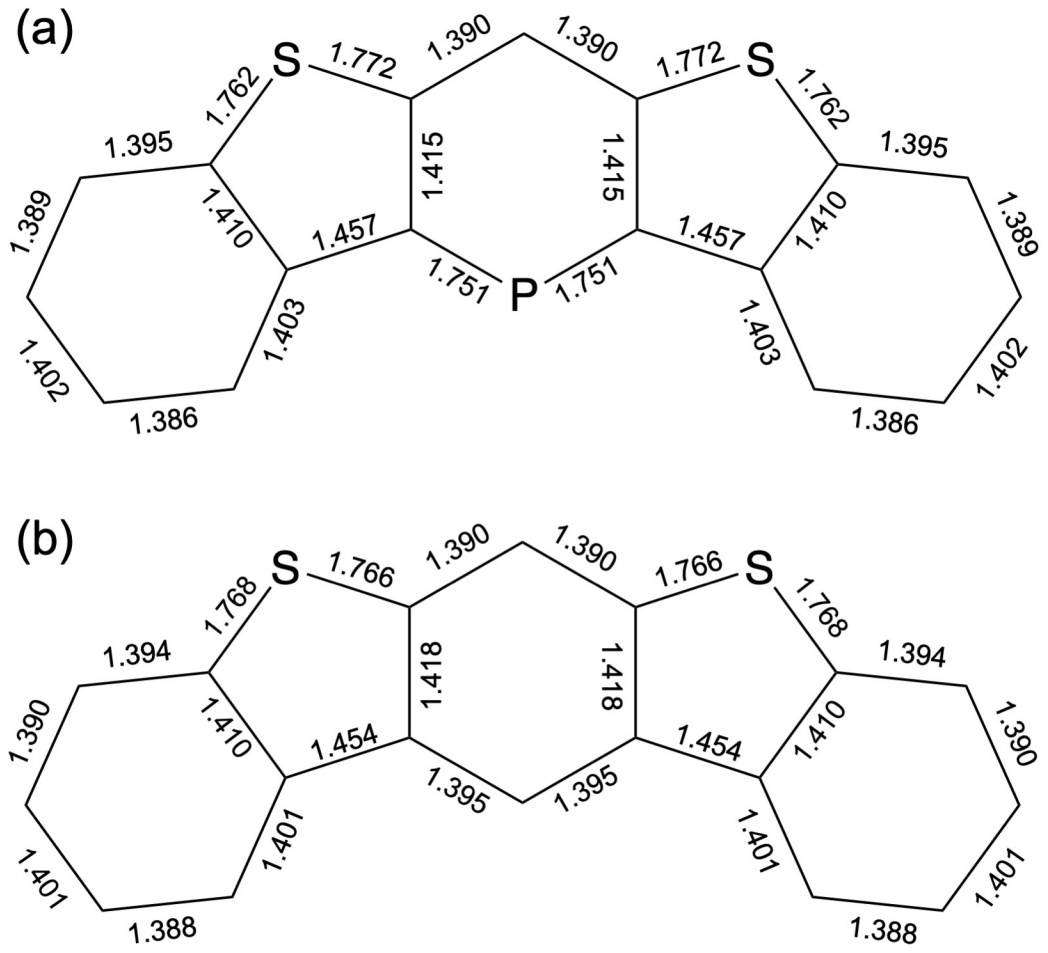

Fig. S6 Bond lengths (Å) of (a) **1** and (b) **4** in the optimized geometries calculated at the B3LYP/6-311G(d,p) level of theory.

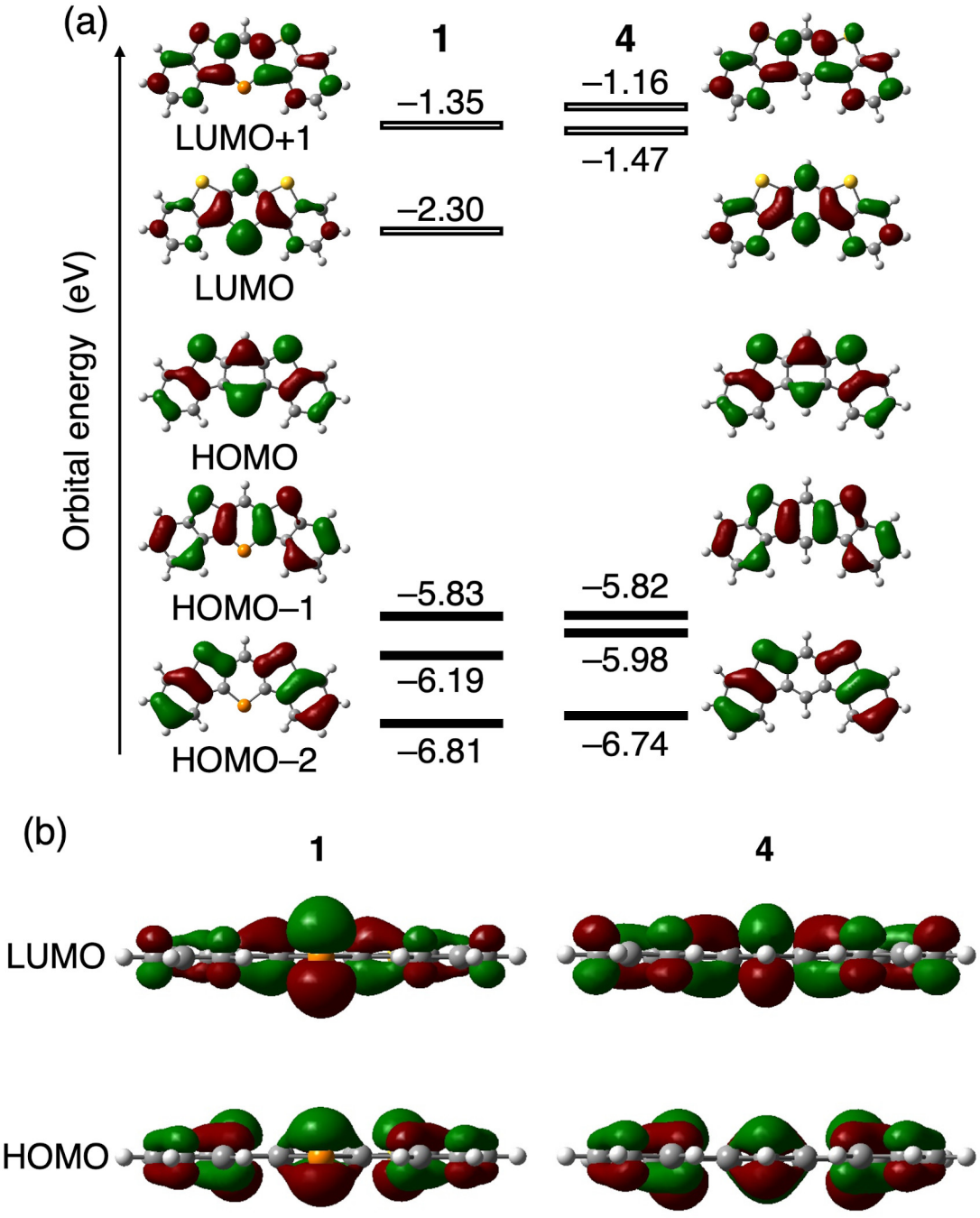

Fig. S7 (a) Orbital energy diagrams and pictorial representations of Kohn–Sham molecular orbitals of **1** and **4** calculated at the B3LYP/6-311G(d,p) level of theory. (b) Side views of HOMO and LUMO.

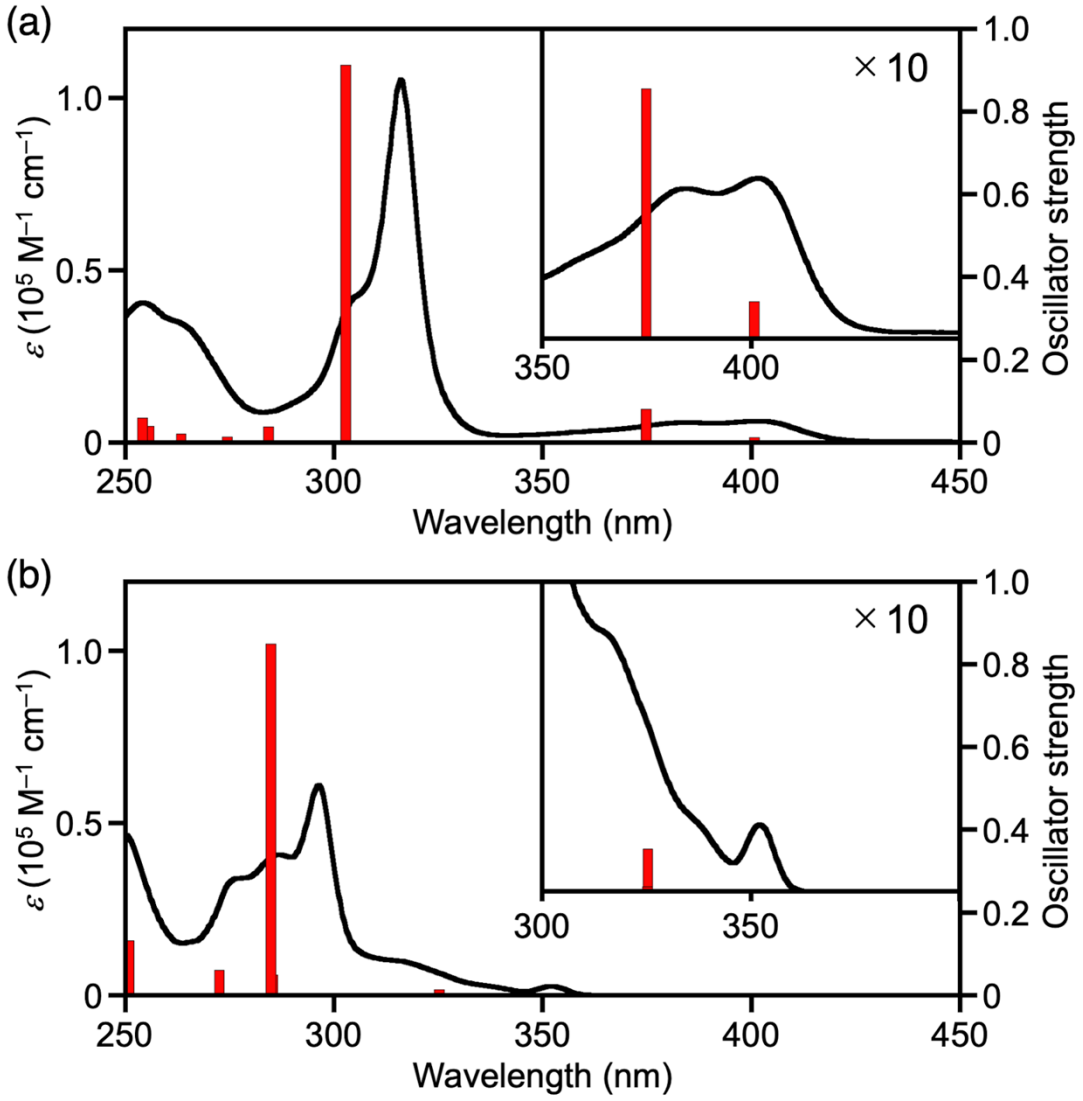

Fig. S8 UV-Vis absorption spectra (black lines) in chloroform and vertical excitation energies and oscillator strength (red line) calculated at the B3LYP/6-311G(d,p) level of theory of (a) **1** and (b) **4**.

Table S1. Main $S_0 \rightarrow S_n$ transitions for **1** and **4** calculated at the B3LYP/6-311G(d,p) level of theory.

	state	E [eV]	λ [nm]	f [-]	Main configuration [%]	
1	S_1	3.0947	401	0.0121	H→L	95
	S_4	4.0954	303	0.9131	H→L+1	72
					H−1→L	11
					H−2→L	11
4	S_1	3.8126	325	0.0138	H−1→L	61
					H→L+1	36
	S_4	4.3527	285	0.8501	H→L+1	58
					H−1→L	35

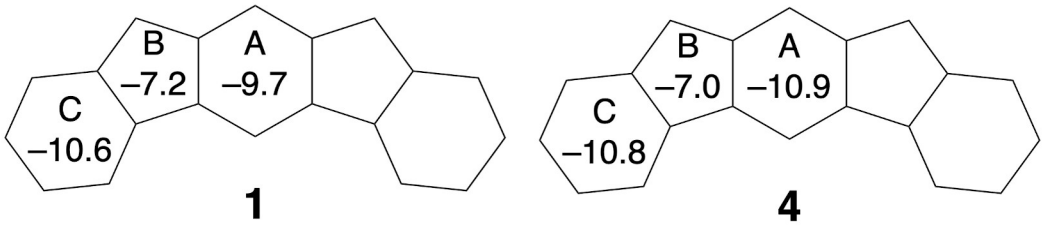

Fig. S9 Calculated NICS(1) values of **1** and **4**.

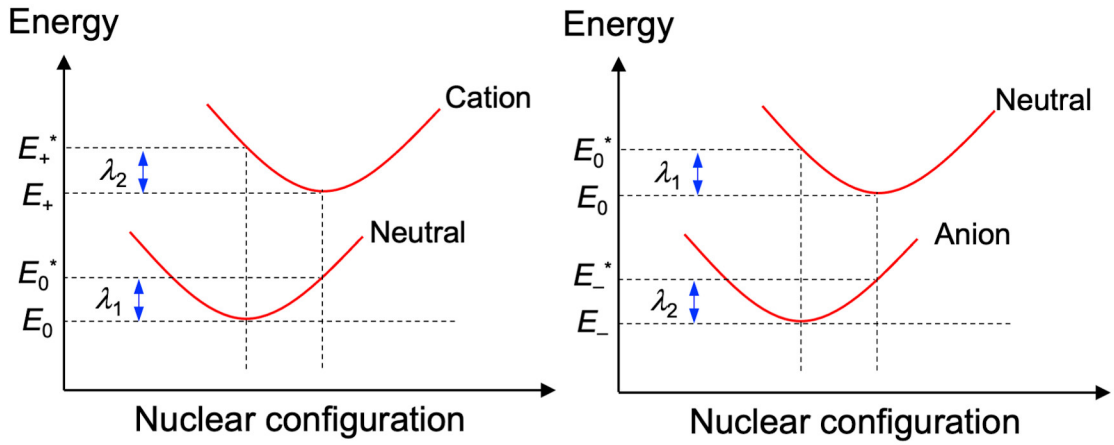

Fig. S10 Schematic diagram for the calculation of the reorganization energy.

Table S2. Reorganization energies of **1** and **4** calculated at the B3LYP/6-311G(d,p) level of theory.

	λ_+ [meV]	λ_- [meV]
1	84	235
4	88	188

Table S3. The Cartesian coordinates (Å) of the optimized geometry for **1** in neutral state at the B3LYP/6-311G(d,p) level of theory.

Atom	X	Y	Z
P	0.000000	0.000000	-1.347821
C	-1.348042	0.000000	-0.230895
C	-1.207840	0.000000	1.176826
C	0.000000	0.000000	1.864767
C	1.207840	0.000000	1.176826
C	1.348042	0.000000	-0.230895
C	-2.748874	0.000000	-0.629913
C	-3.292927	0.000000	-1.923396
C	-4.668583	0.000000	-2.094813
C	-5.526213	0.000000	-0.985954
C	-5.014174	0.000000	0.305075
C	-3.629566	0.000000	0.471737
C	2.748874	0.000000	-0.629913
C	3.292927	0.000000	-1.923396
C	4.668583	0.000000	-2.094813
C	5.526213	0.000000	-0.985954
C	5.014174	0.000000	0.305075
C	3.629566	0.000000	0.471737
S	-2.771400	0.000000	2.010734
S	2.771400	0.000000	2.010734
H	0.000000	0.000000	2.948579
H	-2.634856	0.000000	-2.784938
H	-5.085580	0.000000	-3.095113

H	-6.599815	0.000000	-1.134695
H	-5.676859	0.000000	1.162363
H	2.634856	0.000000	-2.784938
H	5.085580	0.000000	-3.095113
H	6.599815	0.000000	-1.134695
H	5.676859	0.000000	1.162363

Table S4. The Cartesian coordinates (Å) of the optimized geometry for **4** in neutral state at the B3LYP/6-311G(d,p) level of theory.

Atom	X	Y	Z
C	0.000000	0.000000	-0.854370
C	-1.207248	0.000000	-0.155748
C	-1.187247	0.000000	1.262404
C	0.000000	0.000000	1.985882
C	1.187247	0.000000	1.262404
C	1.207248	0.000000	-0.155748
C	-2.563411	0.000000	-0.681393
C	-2.992976	0.000000	-2.014934
C	-4.350269	0.000000	-2.304637
C	-5.298406	0.000000	-1.273505
C	-4.897795	0.000000	0.057366
C	-3.533334	0.000000	0.342069
C	2.563411	0.000000	-0.681393
C	2.992976	0.000000	-2.014934
C	4.350269	0.000000	-2.304637
C	5.298406	0.000000	-1.273505
C	4.897795	0.000000	0.057366
C	3.533334	0.000000	0.342069
S	-2.811072	0.000000	1.955662
S	2.811072	0.000000	1.955662
H	0.000000	0.000000	-1.938546
H	0.000000	0.000000	3.069013
H	-2.266242	0.000000	-2.819622

H	-4.680365	0.000000	-3.336956
H	-6.355502	0.000000	-1.512934
H	-5.631645	0.000000	0.854691
H	2.266242	0.000000	-2.819622
H	4.680365	0.000000	-3.336956
H	6.355502	0.000000	-1.512934
H	5.631645	0.000000	0.854691

Table S5. The Cartesian coordinates (Å) of the optimized geometry for **1** in cation state at the UB3LYP/6-311G(d,p) level of theory.

Atom	X	Y	Z
P	0.000000	0.000000	-1.374329
C	-1.353000	0.000000	-0.248736
C	-1.211335	0.000000	1.155436
C	0.000000	0.000000	1.847417
C	1.211335	0.000000	1.155436
C	1.353000	0.000000	-0.248736
C	-2.742303	0.000000	-0.646456
C	-3.299483	0.000000	-1.936160
C	-4.674196	0.000000	-2.080984
C	-5.527786	0.000000	-0.956341
C	-5.014639	0.000000	0.326869
C	-3.622618	0.000000	0.475193
C	2.742303	0.000000	-0.646456
C	3.299483	0.000000	-1.936160
C	4.674196	0.000000	-2.080984
C	5.527786	0.000000	-0.956341
C	5.014639	0.000000	0.326869
C	3.622618	0.000000	0.475193
S	-2.760405	0.000000	1.985035
S	2.760405	0.000000	1.985035
H	0.000000	0.000000	2.931638

H	-2.658714	0.000000	-2.809785
H	-5.107926	0.000000	-3.073367
H	-6.600915	0.000000	-1.102605
H	-5.669103	0.000000	1.189319
H	2.658714	0.000000	-2.809785
H	5.107926	0.000000	-3.073367
H	6.600915	0.000000	-1.102605
H	5.669103	0.000000	1.189319

Table S6. The Cartesian coordinates (Å) of the optimized geometry for **1** in anion state at the UB3LYP/6-311G(d,p) level of theory.

Atom	X	Y	Z
P	0.000000	0.000000	-1.414652
C	-1.369311	0.000000	-0.235284
C	-1.208275	0.000000	1.156403
C	0.000000	0.000000	1.864711
C	1.208275	0.000000	1.156403
C	1.369311	0.000000	-0.235284
C	-2.756182	0.000000	-0.619143
C	-3.312313	0.000000	-1.916434
C	-4.690818	0.000000	-2.087054
C	-5.556643	0.000000	-0.985621
C	-5.034533	0.000000	0.310831
C	-3.655677	0.000000	0.479112
C	2.756182	0.000000	-0.619143
C	3.312313	0.000000	-1.916434
C	4.690818	0.000000	-2.087054
C	5.556643	0.000000	-0.985621
C	5.034533	0.000000	0.310831
C	3.655677	0.000000	0.479112
S	-2.778121	0.000000	2.008207
S	2.778121	0.000000	2.008207

H	0.000000	0.000000	2.947560
H	-2.650244	0.000000	-2.775034
H	-5.104246	0.000000	-3.091242
H	-6.631238	0.000000	-1.135041
H	-5.695787	0.000000	1.171271
H	2.650244	0.000000	-2.775034
H	5.104246	0.000000	-3.091242
H	6.631238	0.000000	-1.135041
H	5.695787	0.000000	1.171271

Table S7. The Cartesian coordinates (Å) of the optimized geometry for **4** in cation state at the UB3LYP/6-311G(d,p) level of theory.

Atom	X	Y	Z
C	0.000000	0.000000	-0.881902
C	-1.212304	0.000000	-0.180713
C	-1.189896	0.000000	1.233553
C	0.000000	0.000000	1.963540
C	1.189896	0.000000	1.233553
C	1.212304	0.000000	-0.180713
C	-2.561973	0.000000	-0.700740
C	-3.009569	0.000000	-2.027511
C	-4.371072	0.000000	-2.285219
C	-5.313828	0.000000	-1.236083
C	-4.905754	0.000000	0.084490
C	-3.529504	0.000000	0.344746
C	2.561973	0.000000	-0.700740
C	3.009569	0.000000	-2.027511
C	4.371072	0.000000	-2.285219
C	5.313828	0.000000	-1.236083
C	4.905754	0.000000	0.084490
C	3.529504	0.000000	0.344746
S	-2.797255	0.000000	1.925641

S	2.797255	0.000000	1.925641
H	0.000000	0.000000	-1.965602
H	0.000000	0.000000	3.046901
H	-2.302405	0.000000	-2.848074
H	-4.721361	0.000000	-3.310120
H	-6.371311	0.000000	-1.469537
H	-5.627511	0.000000	0.891553
H	2.302405	0.000000	-2.848074
H	4.721361	0.000000	-3.310120
H	6.371311	0.000000	-1.469537
H	5.627511	0.000000	0.891553

Table S8. The Cartesian coordinates (Å) of the optimized geometry for **4** in anion state at the UB3LYP/6-311G(d,p) level of theory.

Atom	X	Y	Z
C	0.000000	0.000000	-0.891632
C	-1.225532	0.000000	-0.166780
C	-1.191189	0.000000	1.243231
C	0.000000	0.000000	1.981082
C	1.191189	0.000000	1.243231
C	1.225532	0.000000	-0.166780
C	-2.570517	0.000000	-0.670320
C	-3.019226	0.000000	-2.015189
C	-4.378652	0.000000	-2.295476
C	-5.335623	0.000000	-1.269945
C	-4.918324	0.000000	0.071093
C	-3.560623	0.000000	0.348841
C	2.570517	0.000000	-0.670320
C	3.019226	0.000000	-2.015189
C	4.378652	0.000000	-2.295476
C	5.335623	0.000000	-1.269945
C	4.918324	0.000000	0.071093

C	3.560623	0.000000	0.348841
S	-2.816105	0.000000	1.953225
S	2.816105	0.000000	1.953225
H	0.000000	0.000000	-1.974137
H	0.000000	0.000000	3.063856
H	-2.294328	0.000000	-2.821736
H	-4.708944	0.000000	-3.330624
H	-6.393898	0.000000	-1.507890
H	-5.646879	0.000000	0.875439
H	2.294328	0.000000	-2.821736
H	4.708944	0.000000	-3.330624
H	6.393898	0.000000	-1.507890
H	5.646879	0.000000	0.875439

Table S9. Calculated charge transfer integrals of LUMOs for **1** and **4**.

	t_1 [meV]	t_2 [meV]	t_3 [meV]	t_4 [meV]	t_5 [meV]
1	100.6	10.5	24.0	2.8	8.6
4	38.1	8.3	16.1	-	-

8. Time-resolved microwave conductivity measurements

TRMC measurement was performed for the crystalline powdery samples of **1** and **4** prepared by vacuum sublimation. Samples were fixed on a quartz substrate by adhesive tape. Transient charge carriers were generated through photoexcitation by laser pulses of third harmonic generation (λ = 355 nm) from a Nd:YAG laser with a pulse duration of 5–8 ns at the photon density of 9.1×10^{15} photon cm^{-2}. The frequency and power of probing microwave were set at around 9.1 GHz and 3 mW, respectively. Photoconductivity transients, demodulated through a GaAs crystal–diode with Schottky–barriers (rise time < 1 ns), were monitored by a Tektronix model DPO4104 digital oscilloscope through a microwave amplifier and diode (rise time < 1 ns). The photoconductivity ($\Delta\sigma = A^{-1}\,\Delta P_r\,P_r^{-1}$ where A is the sensitivity factor, P_r is the reflected microwave power, and ΔP_r is the change in P_r upon exposure to light) was converted into the product of the quantum yield (ϕ) and sum of the charge carrier mobilities $\Sigma\mu$ ($= \mu_+ + \mu_-$) using the relationship $\phi\Sigma\mu = \Delta\sigma(eI_0F_{light})^{-1}$, where e and F_{Light} are the electron charge and correction (or filling) factor, respectively. The experiments were performed at room temperature in the air.

9. Fabrication and evaluation of organic field-effect transistors

The OFET devices with a bottom-gate bottom-contact configuration were fabricated. The p-doped silicon substrate functions as the gate electrode. A thermally grown silicon oxide (SiO_2) dielectric layer on the gate substrate was 300 nm thick with a capacitance of 10.0 nF cm^{-2}. Interdigital source and drain electrodes were constructed with gold (30 nm) that were formed on the SiO_2 layer. The channel width (W) and channel length (L) were 294 mm and 25 μm, respectively. The SiO_2 surface was washed with toluene, acetone, water, and 2-propanol for 15 min each in an ultrasonic bath. Substrates were dried with a flow of N_2 gas, and the SiO_2 surface was then activated by UV–O_3 cleaner (Filgen UV253V8) for 45 min. The active layer was prepared by drop-cast method using 0.6 and 1.0 g L^{-1} $CHCl_3$ solution for **1** and **4**, respectively, in N_2 glove box. The output and transfer characteristics of the OFETs were measured by using a KEITHLEY 4200SCS semiconductor parameter analyzer at room temperature under a N_2 glove box. The field-effect mobilities (μ) were determined from the transfer curve in the saturation regime at the V_{DS} of –100 V using the following equation,

$$I_{DS} = (\mu W C_i / 2L)(V_G - V_{th})^2$$

where I_{DS} is the drain–source current and V_{DS}, V_G, and V_{th} are the drain–source voltage, gate voltage, and threshold voltage, respectively. The on/off current ratios (I_{on}/I_{off}) were determined from the I_{DS} at V_G = 0 V (I_{off}) and V_G = –100 V (I_{on}).

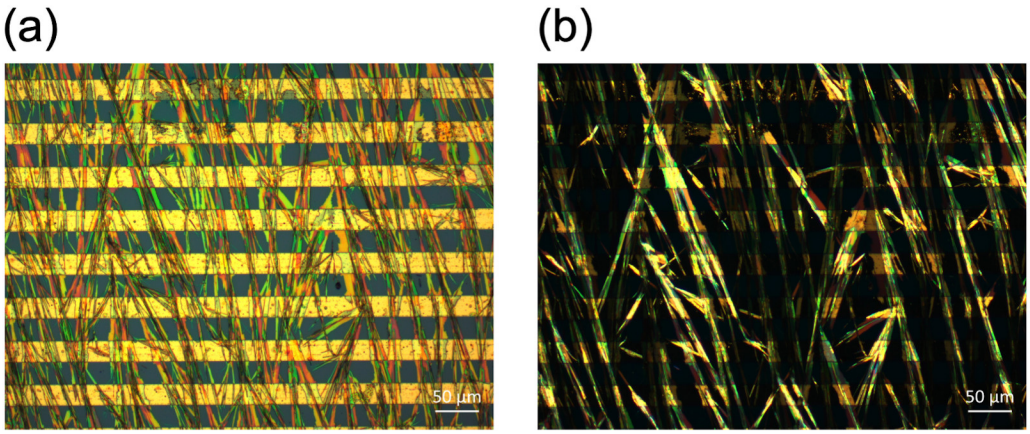

Fig. S11 Optical micrographs of the OFET of **1** (a) without and (b) with the polarizing filter.

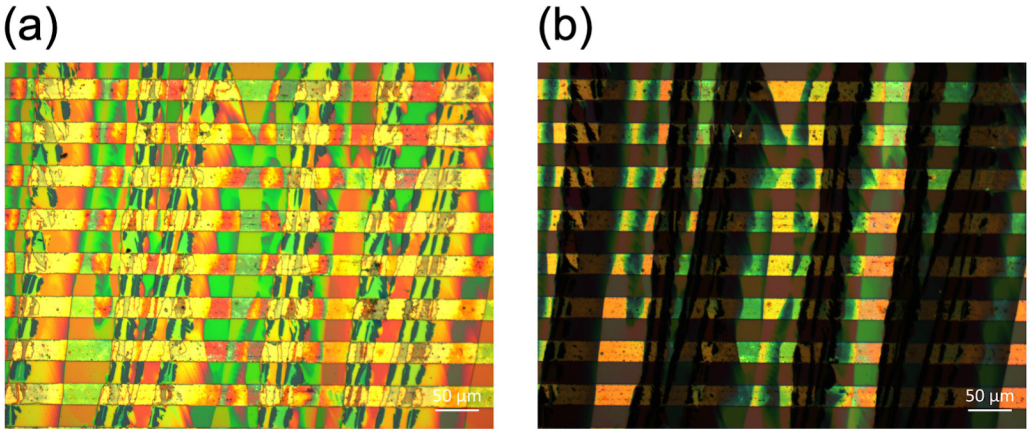

Fig. S12 Optical micrographs of the OFET of **4** (a) without and (b) with the polarizing filter.

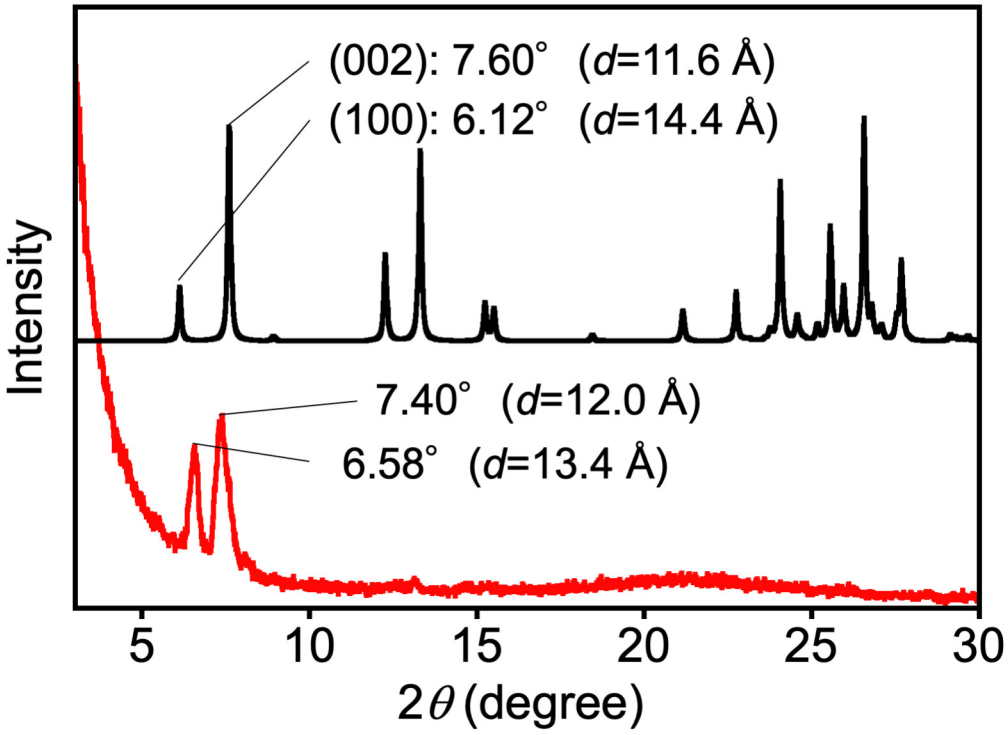

Fig. S13 Out-of-plane X-ray diffraction patterns of OFET of **1** (red) and simulated pattern from the single crystal structure (black).

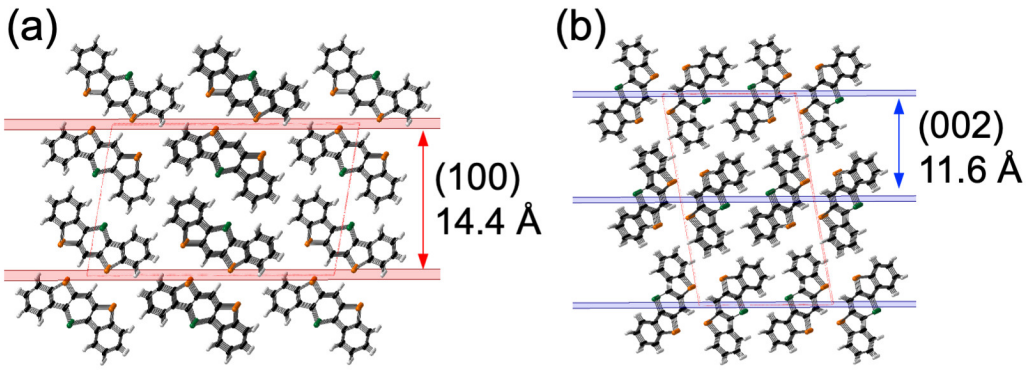

Fig. S14 Packing structure of **1** displaying (a) (100) and (b) (002) lattice planes.

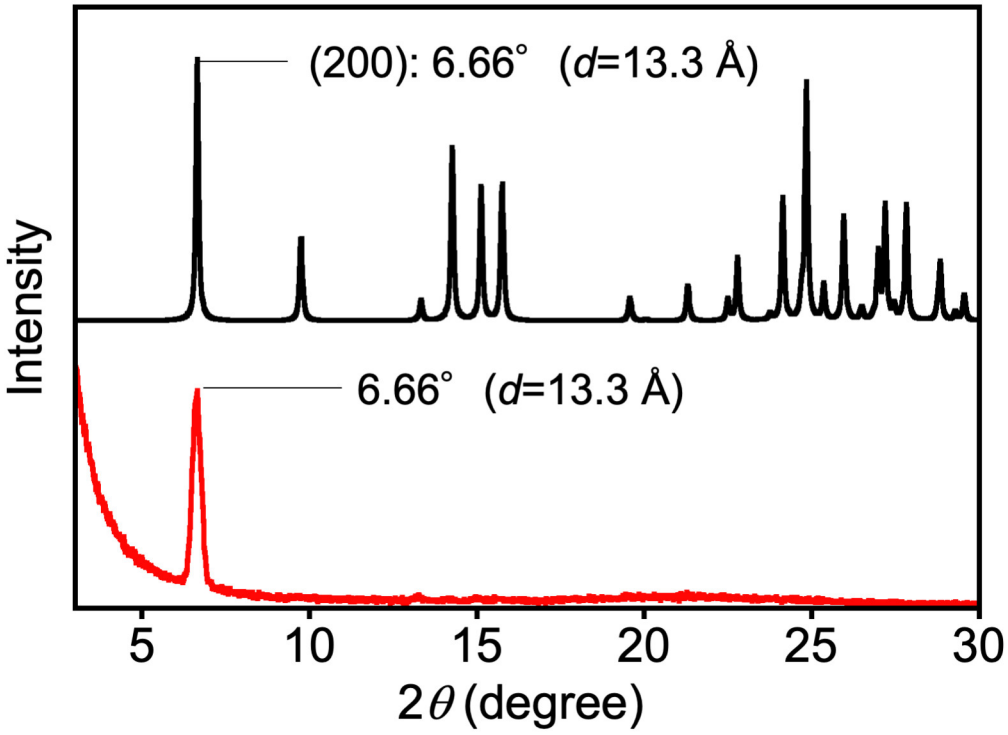

Fig. S15 Out-of-plane X-ray diffraction patterns of OFET of **4** (red) and simulated pattern from the single crystal structure (black).

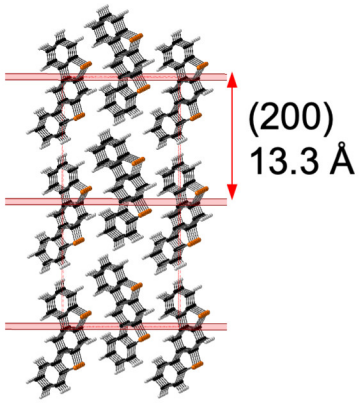

Fig. S16 Packing structure of **4** displaying (200) lattice planes.

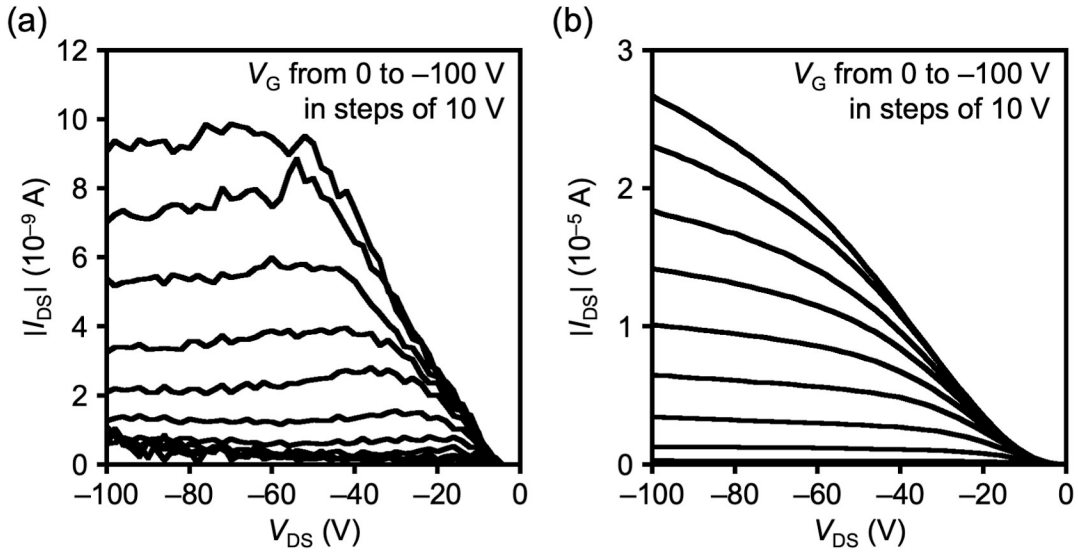

Fig. S17 Output characteristics of the OFETs based on (a) **1** and (b) **4**.

10. ^{1}H, ^{13}C, and ^{31}P NMR spectral data

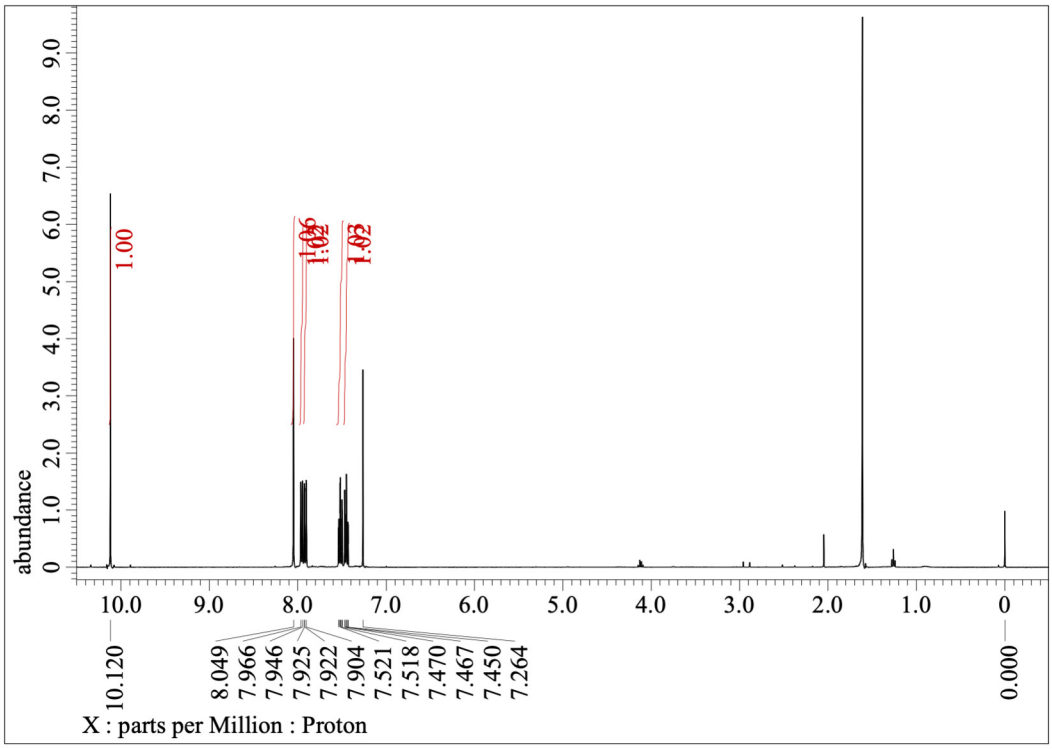

Fig. S18 ^{1}H NMR spectrum of **5** in $CDCl_3$ (400 MHz).

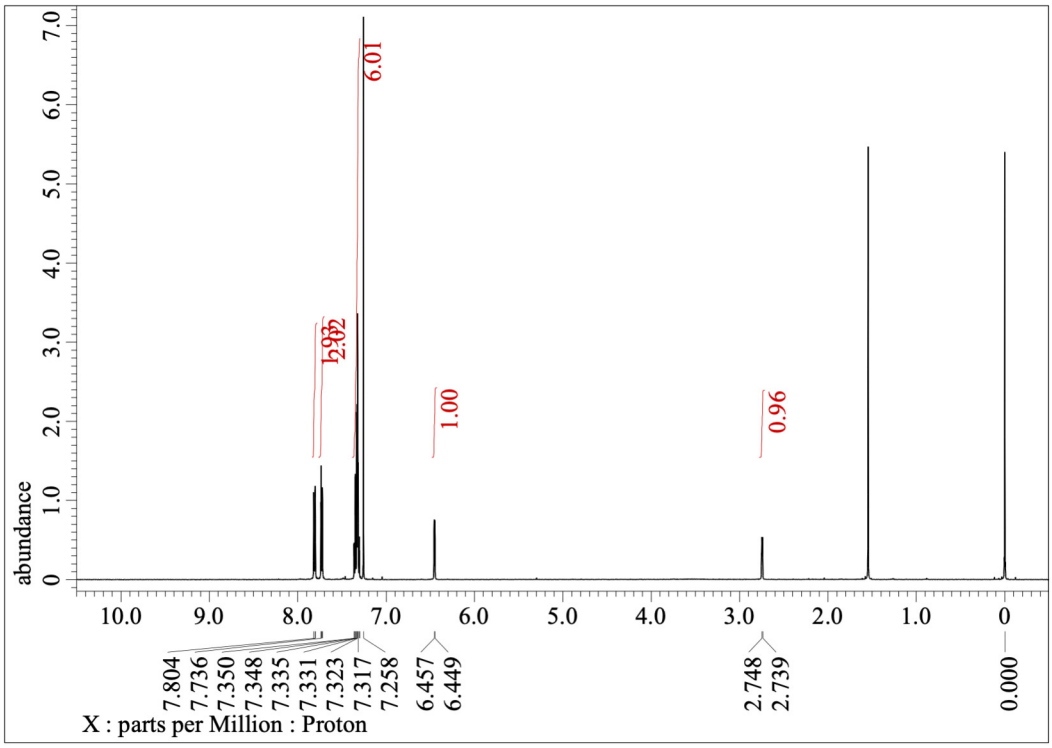

Fig. S19 ^{1}H NMR spectrum of **6** in $CDCl_3$ (500 MHz).

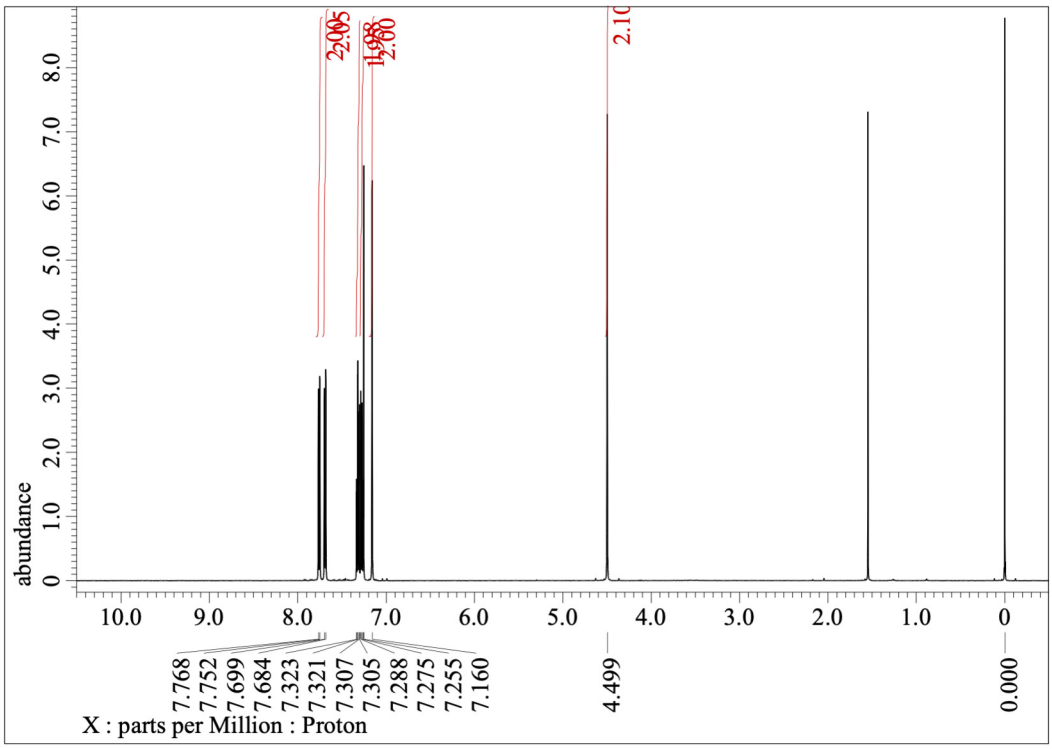

Fig. S20 ^{1}H NMR spectrum of **2** in $CDCl_3$ (500 MHz).

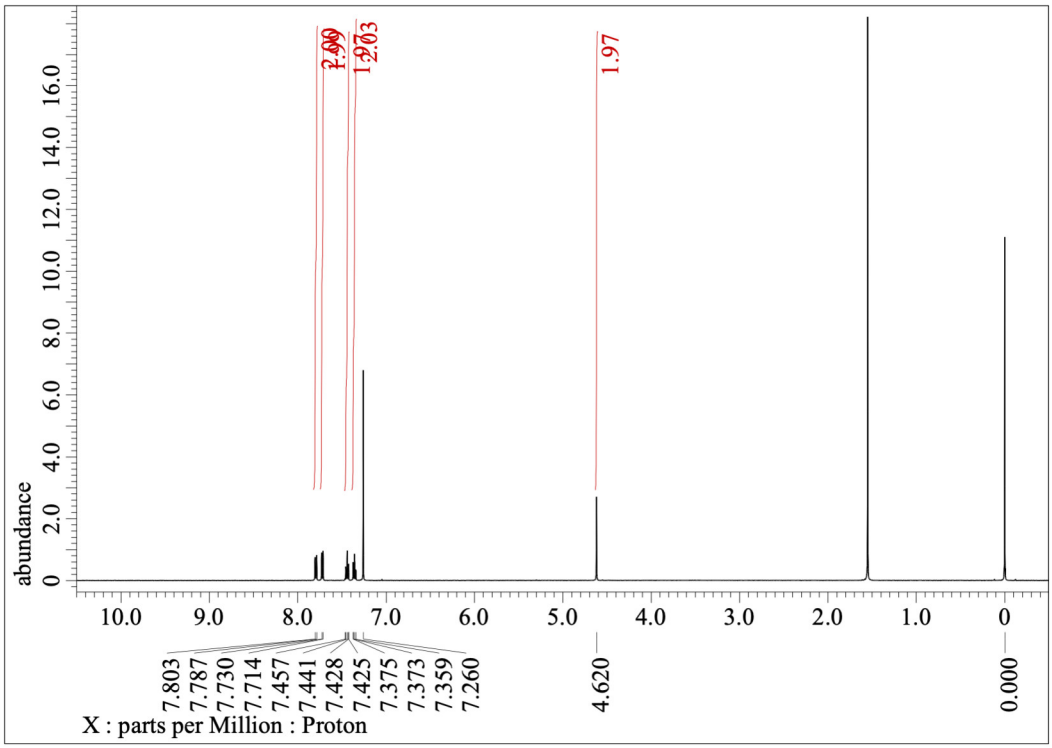

Fig. S21 ^{1}H NMR spectrum of **3** in $CDCl_3$ (500 MHz).

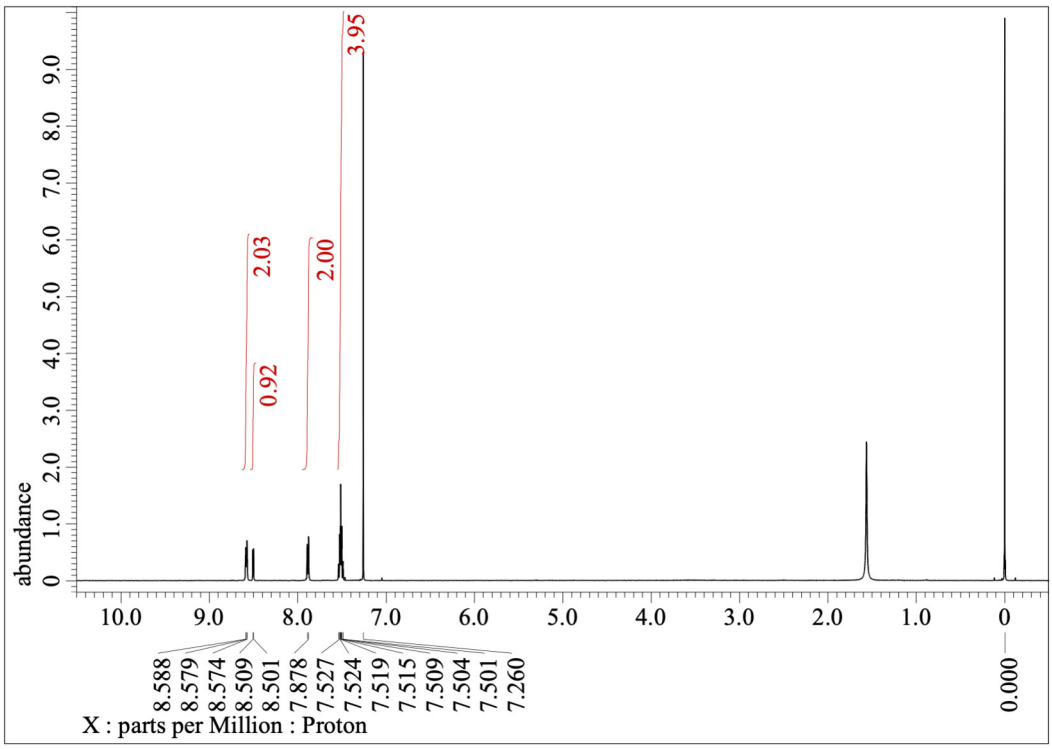

Fig. S22 ^{1}H NMR spectrum of **1** in $CDCl_3$ (500 MHz).

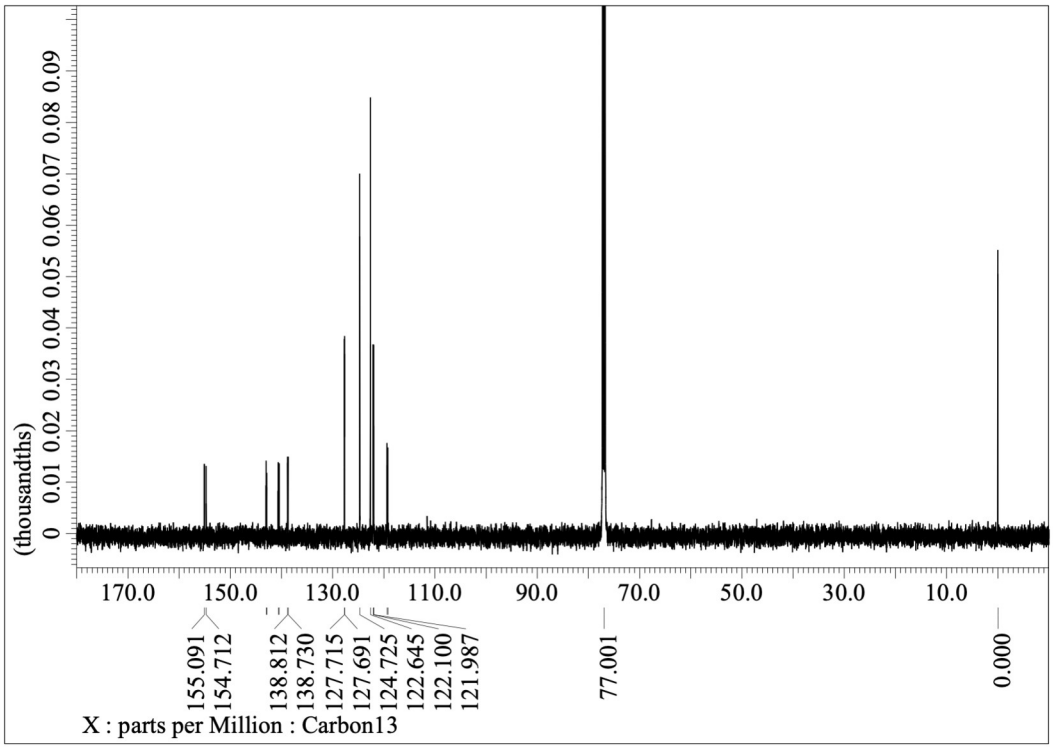

Fig. S23 ^{13}C NMR spectrum of **1** in $CDCl_3$ (126 MHz).

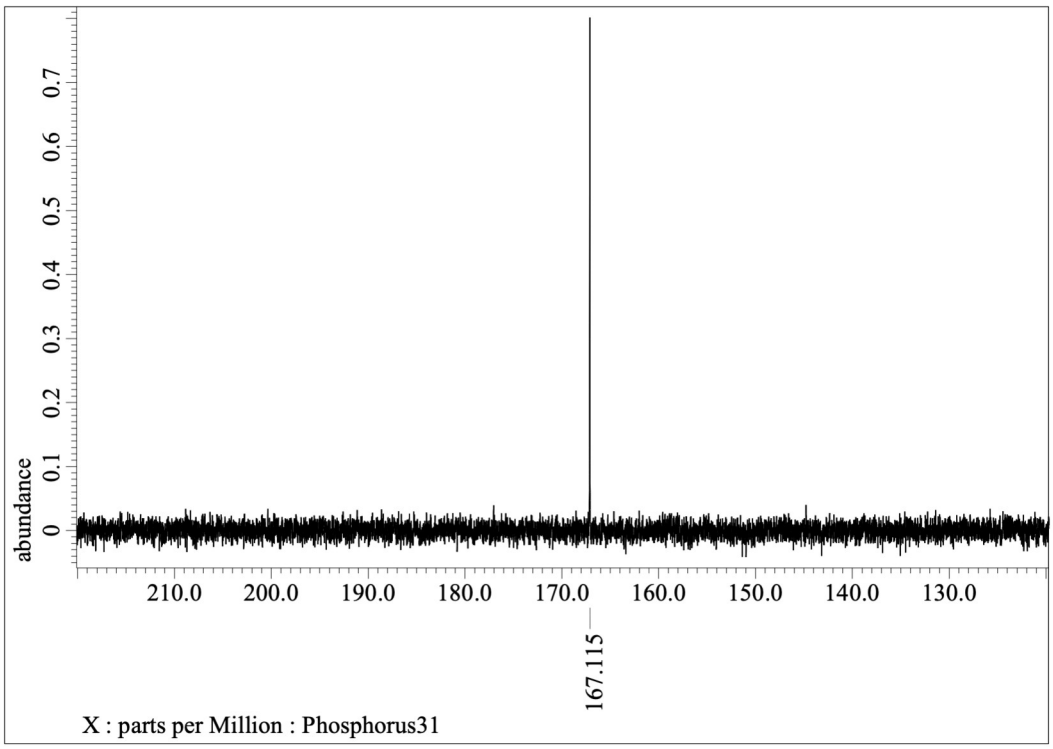

Fig. S24 ^{31}P NMR spectrum of **1** in $CDCl_3$ (202 MHz).

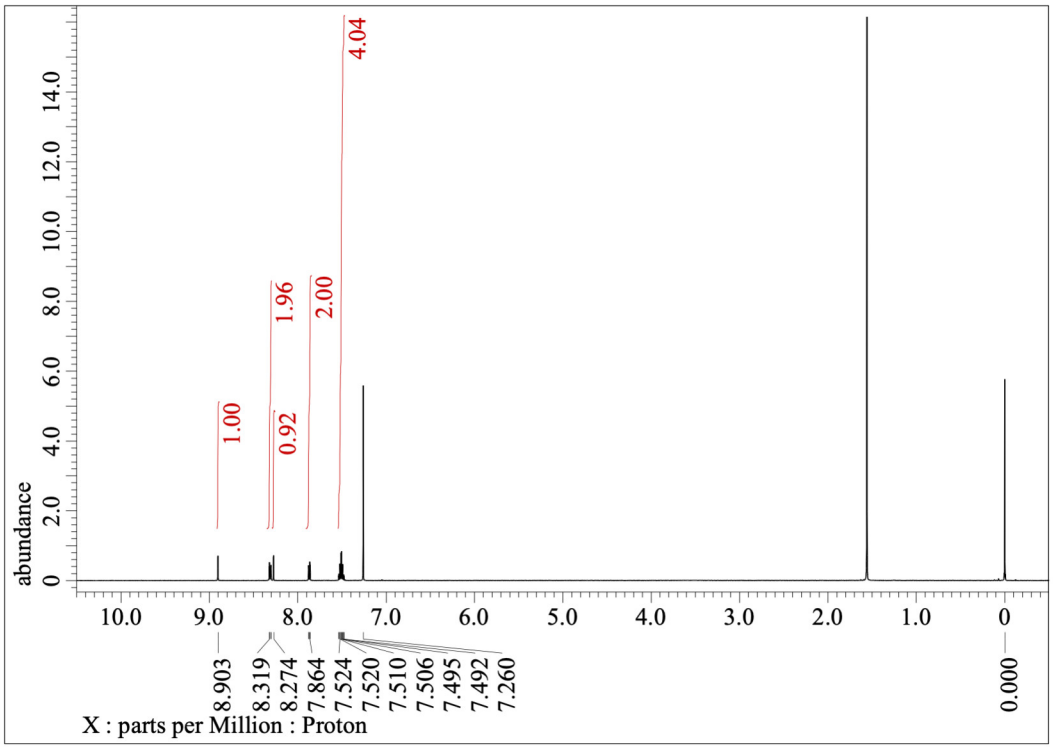

Fig. S25 ^{1}H NMR spectrum of **4** in $CDCl_3$ (500 MHz).

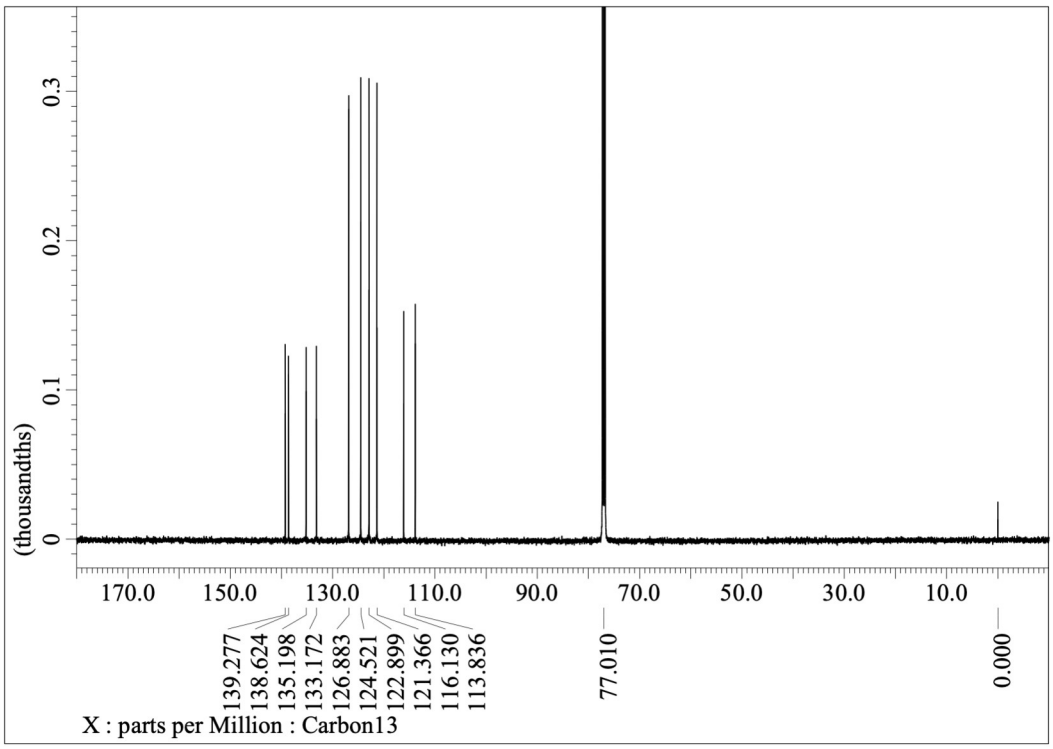

Fig. S26 ^{13}C NMR spectrum of **4** in $CDCl_3$ (126 MHz).

11. HR-Mass data

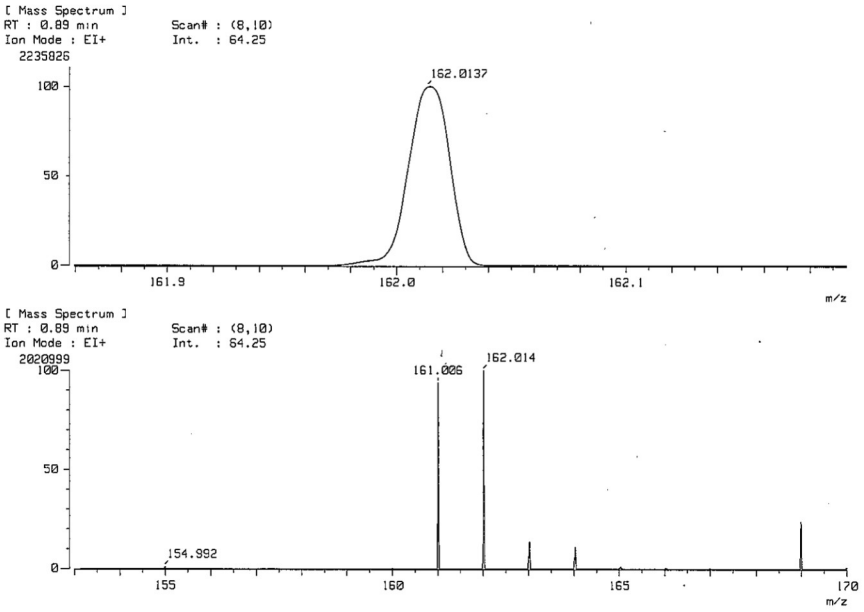

Fig. S27 HR-EI mass spectra of **5**.

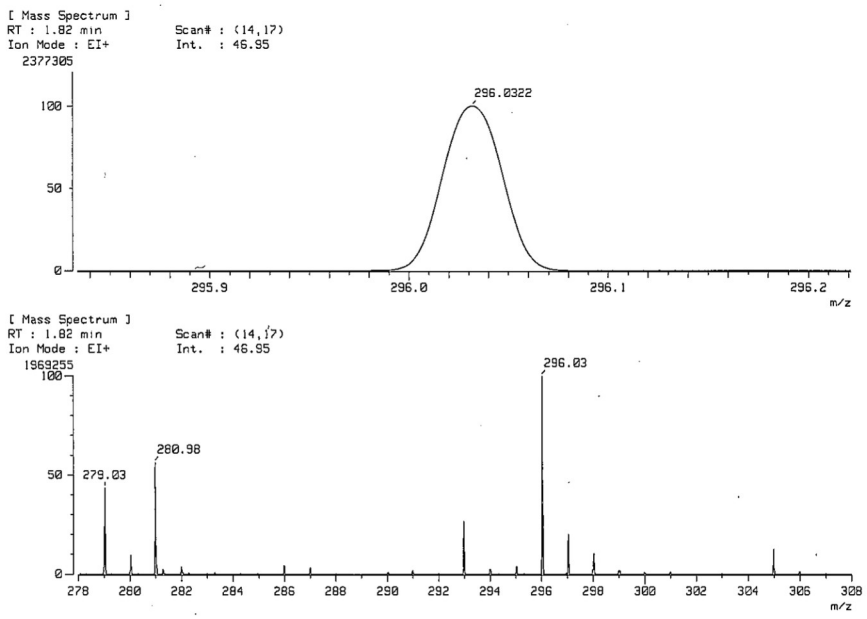

Fig. S28 HR-EI mass spectra of **6**.

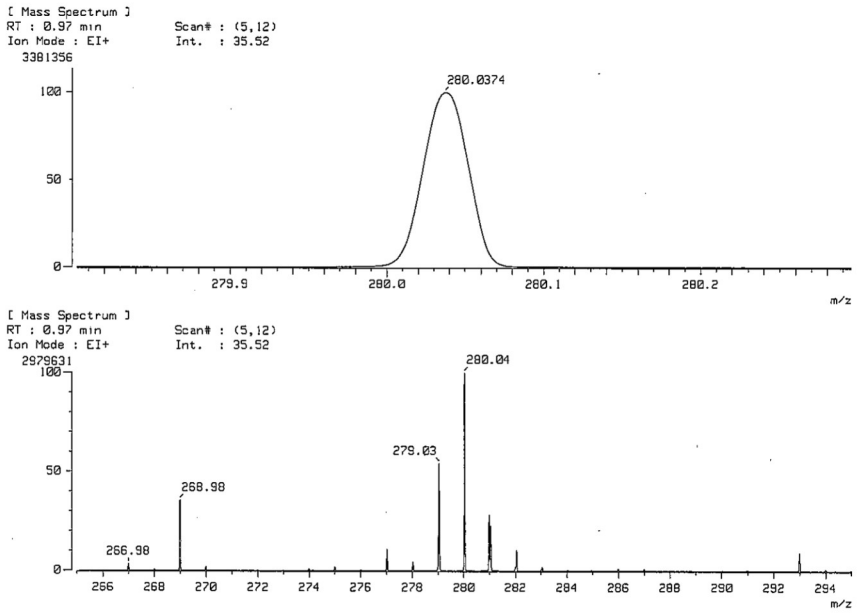

Fig. S29 HR-EI mass spectra of **2**.

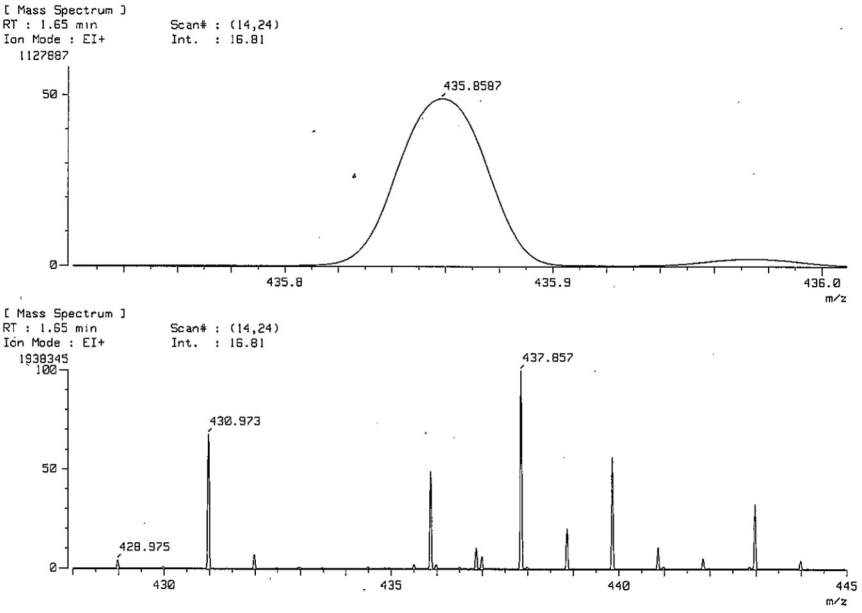

Fig. S30 HR-EI mass spectra of **3**.

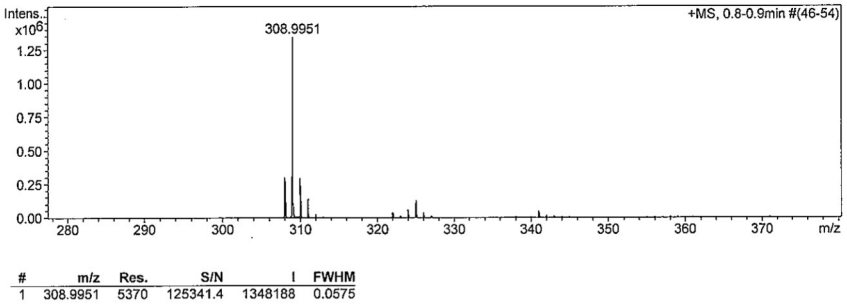

#	m/z	Res.	S/N	I	FWHM
1	308.9951	5370	125341.4	1348188	0.0575

Fig. S31 HR-APCI-TOF mass spectrum of **1**.

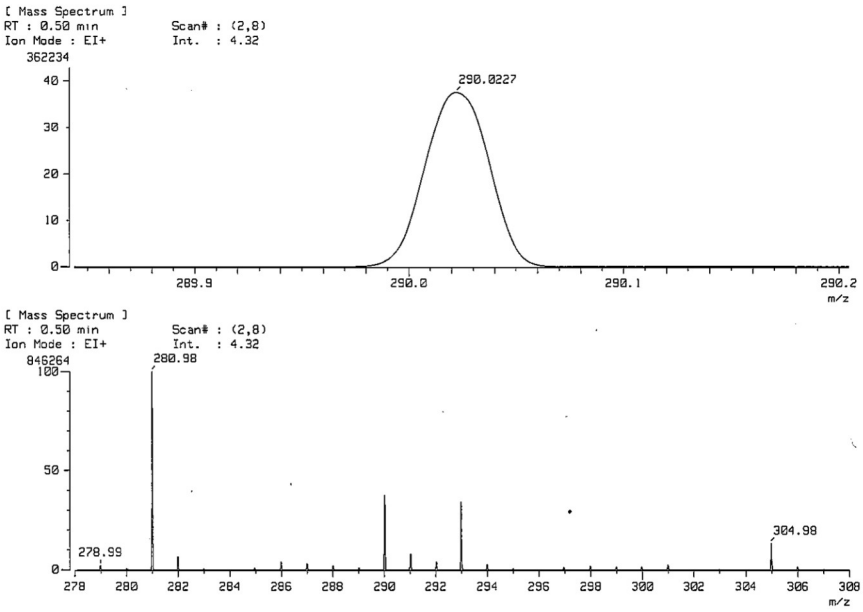

Fig. S32 HR-EI mass spectra of **4**.

12. References

[S1] N. Gigant, E. Claveau, P. Bouyssou and I. Gillaizeau, *Org. Lett*., 2012, **14**, 844–847.

[S2] V. G. Nenajdenko, I. L. Baraznenok and E. S. Balenkova, *J. Org. Chem.*, 1998, **63**, 6132–6136.

[S3] L. E. Doyle, W. E. Piers and J. Borau-Garcia, *J. Am. Chem. Soc.*, 2015, **137**, 2187−2190.

[S4] G. M. Sheldrick, *Acta Cryst. Sec. C*, 2015, **71**, 3–8.

[S5] Gaussian 16, Revision C.01, M. J. Frisch, G. W. Trucks, H. B. Schlegel, G. E. Scuseria, M. A. Robb, J. R. Cheeseman, G. Scalmani, V. Barone, G. A. Petersson, H. Nakatsuji, X. Li, M. Caricato, A. V. Marenich, J. Bloino, B. G. Janesko, R. Gomperts, B. Mennucci, H. P. Hratchian, J. V. Ortiz, A. F. Izmaylov, J. L. Sonnenberg, D. Williams-Young, F. Ding, F. Lipparini, F. Egidi, J. Goings, B. Peng, A. Petrone, T. Henderson, D. Ranasinghe, V. G. Zakrzewski, J. Gao, N. Rega, G. Zheng, W. Liang, M. Hada, M. Ehara, K. Toyota, R. Fukuda, J. Hasegawa, M. Ishida, T. Nakajima, Y. Honda, O. Kitao, H. Nakai, T. Vreven, K. Throssell, J. A. Montgomery, Jr., J. E. Peralta, F. Ogliaro, M. J. Bearpark, J. J. Heyd, E. N. Brothers, K. N. Kudin, V. N. Staroverov, T. A. Keith, R. Kobayashi, J. Normand, K. Raghavachari, A. P. Rendell, J. C. Burant, S. S. Iyengar, J. Tomasi, M. Cossi, J. M. Millam, M. Klene, C. Adamo, R. Cammi, J. W. Ochterski, R. L. Martin, K. Morokuma, O. Farkas, J. B. Foresman and D. J. Fox, Gaussian, Inc., Wallingford CT, 2019.

[S6] P. von R. Schleyer, C. Maerker, A. Dransfeld, H. Jiao and N. J. R. van Eikema Hommes, *J. Am. Chem. Soc.*, 1996, **118**, 6317–6318.

[S7] G. R. Hutchison, M. A. Ratner and T. J. Marks, *J. Am. Chem. Soc.*, 2005, **127**, 2339–2350.

[S8] ADF2020, SCM, Theoretical Chemistry. Vrije Universiteit, Amsterdam, The Netherlands, http://www.scm.com.